nature reviews earth & environment

https://doi.org/10.1038/s43017-025-00705-7

Supplementary information

Climate impacts of the El Niño–Southern Oscillation in Africa

In the format provided by the authors and unedited

Supplementary Figures

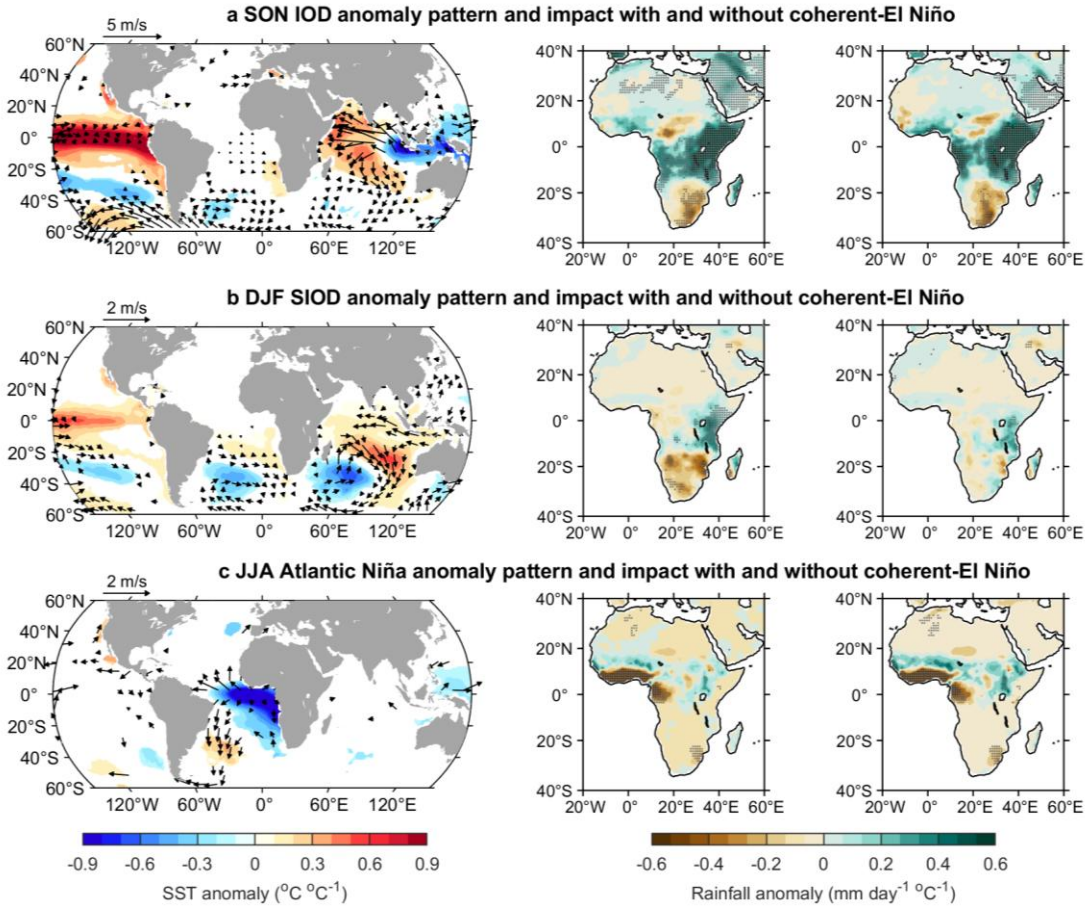

Supplementary Fig. 1 | ENSO impact exerted through modes of interannual variability in the Indian and Atlantic Oceans. a, Observed SON SST and wind (left), rainfall anomaly pattern associated with the Indian Ocean Dipole (IOD) (middle), and rainfall anomaly pattern after ENSO is removed from index of the IOD (right). Shown are regression coefficients onto their respective concurrent indices in their peak seasons using data since 1948. For SST and winds, only statistically significant coefficients above the 95% confidence level are shown, and for rainfall significance above the 95% confidence level is indicated by stipples**. b-c,** The same as **a**, but for a negative phase of the Subtropical Indian Ocean Dipole (SIOD) (DJF) and Atlantic Niña (JJA). ENSO impact can be conducted through other modes of variability, forced by or independent from ENSO, including in the Atlantic and Indian Oceans. The Atlantic Niño/Niña and the IOD has a strong independent component, but the SIOD has little independent component.

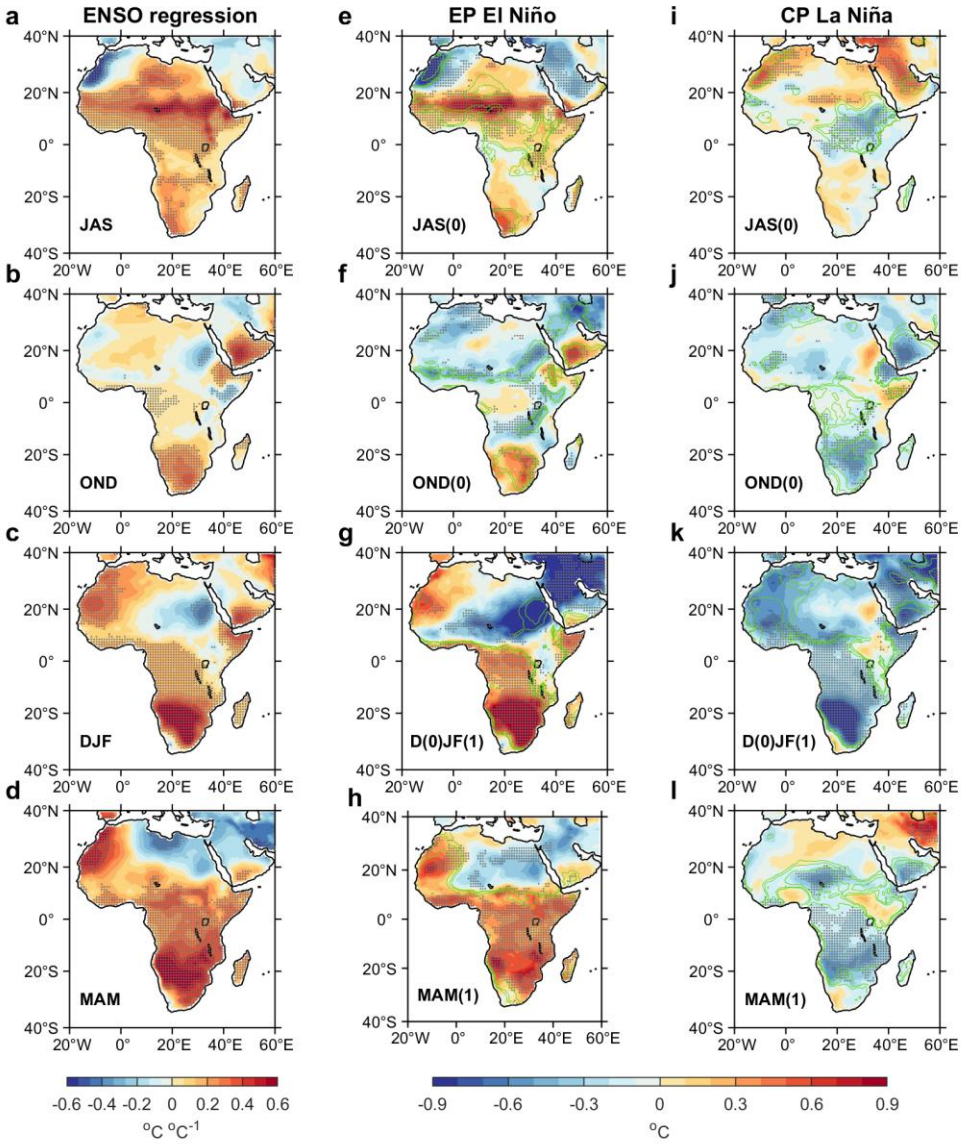

Supplementary Fig. 2. | EP and CP ENSO impacts on African surface air temperatures. a, Observed E-index of December-January-February (DJF)-averaged sea-surface temperature anomalies from 1948 to 2023. An EP El Niño is defined when the E-index is greater than 1.0 standard deviation (s.d.) (red circles in **a**) and an EP La Niña when the E-index is greater than -1.0 s.d. in amplitude (yellow circles in **a**). **b,** Same as **a,** but for C-index. A CP El Niño is defined when the C-index is greater than 1.00 standard deviation (s.d.) (purple circles in **b**) and a CP La Niña when the C-index is greater than -1.0 s.d. in amplitude (blue circles in **b**). **c-f,** Composites of 2m air temperature anomalies (shading) for EP El Niño (left), EP La Niña (middle-left), CP El Niño (middle-right) and CP La Niña (right) during July-August-September (JAS; part **c**), October-November-December (OND; part **d**), December-January-February (DJF; part **e**) and March-April-May (MAM; part **f**). Year 0 in parentheses indicates an El Niño developing year and year 1 the subsequent decaying year. Green contours in parts **c-f**

represent the 90%, 95% and 99% confidence levels. Stippled areas indicate that more than 70% of events have the same-signed anomalies. The opposite impact between El Niño and La Niña is mostly due to that between EP El Niño and CP La Niña.

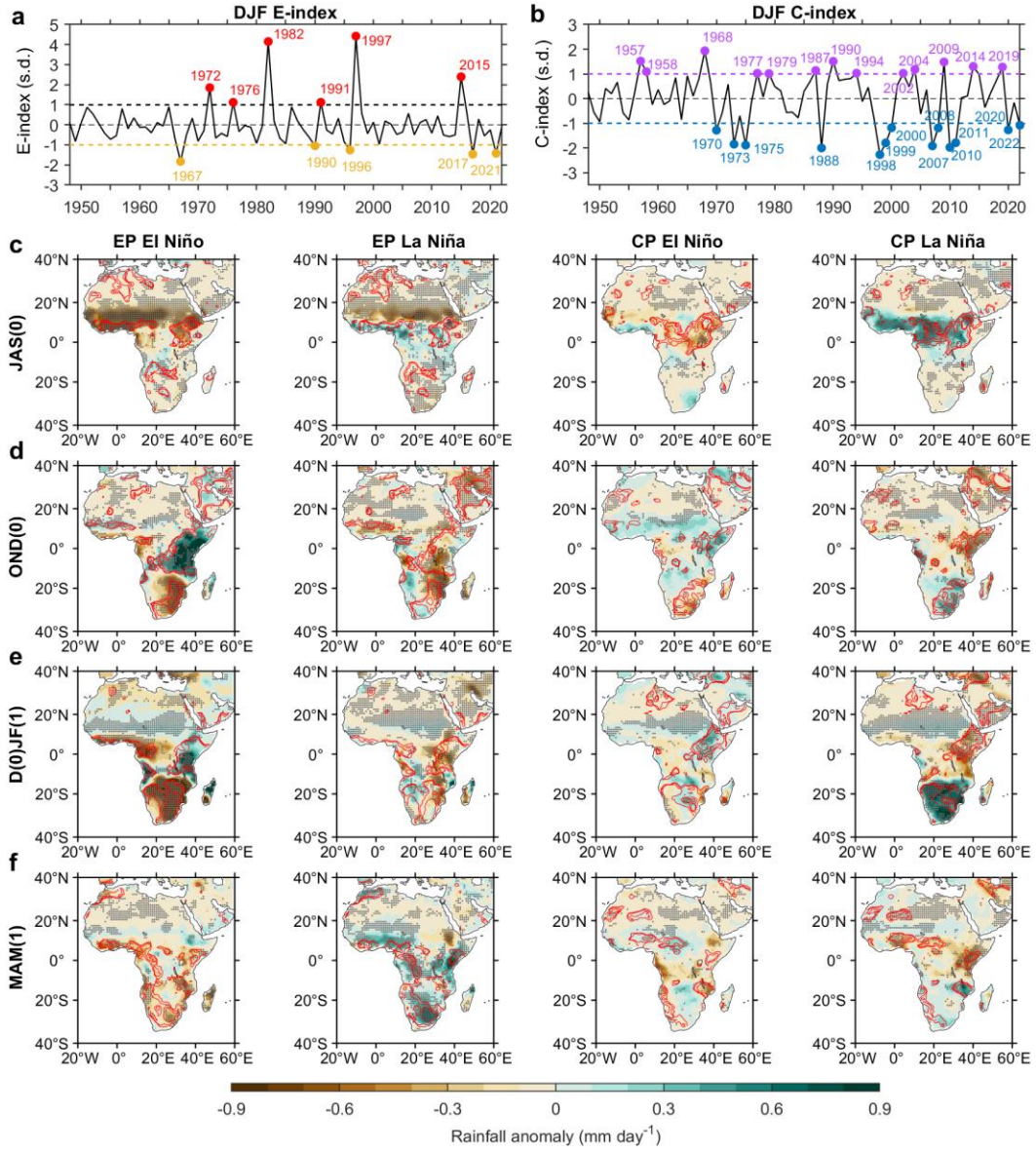

Fig. 3 | EP and CP ENSO impacts on African rainfall. a, Observed E-index of December-January-February (DJF)-averaged SST anomalies since 1948. An EP El Niño is defined when the E-index is greater than 1.00 standard deviation (s.d.) (red circles in **a**) and an EP La Niña when the E-index is greater than -1 s.d. in amplitude (yellow circles in **a**). **b,** Same as **a,** but for C-index. A CP El Niño is defined when the C-index is greater than 1.00 standard deviation (s.d.) (purple circles in **b**) and a CP La Niña when the C-index is greater than -1 s.d. in amplitude (blue circles in **b**). **c-f,** Composites of rainfall (shading) anomalies for EP El Niño (left), EP La Niña (middle-left), CP El Niño (middle-right) and CP La Niña (right) during July-August-September (JAS; part **c**), October-November-December (OND; part **d**), December-January-

February (DJF; part **e**) and March-April-May (MAM; part **f**). Year 0 in parentheses indicates an El Niño developing year and year 1 the subsequent decaying year. Red contours in parts **c-f** represent the 90%, 95% and 99% confidence levels. Stippled areas indicate that more than 70% of events have the same-signed anomalies. An EP El Niño generally exerts a stronger impact than a CP El Niño, but a CP La Niña generally has a stronger influence than an EP La Niña. In addition, the opposite impact between El Niño and La Niña is mostly due to that between EP El Niño and CP La Niña.

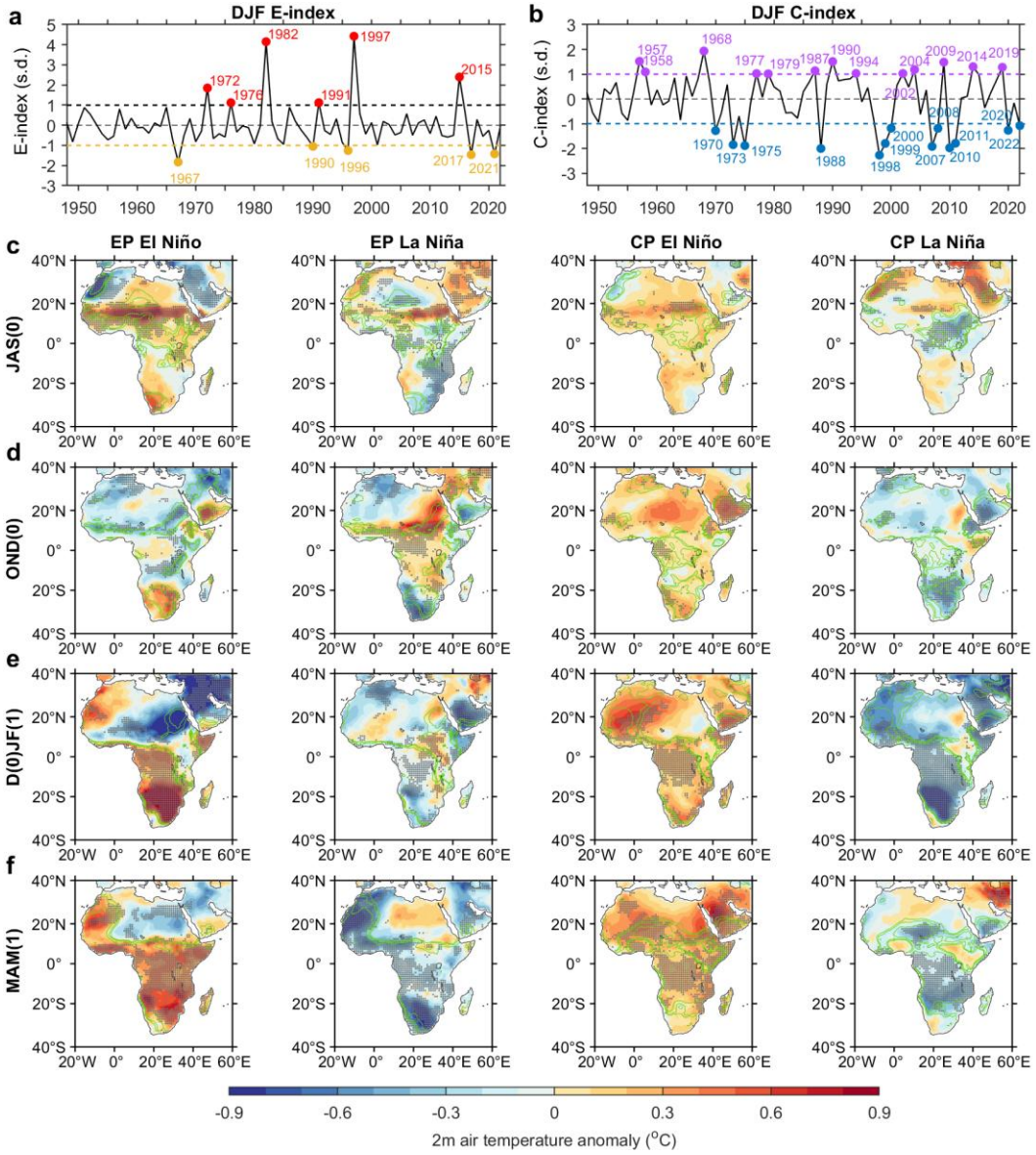

Supplementary Fig. 4. | EP and CP ENSO impacts on African surface air temperature. a, Observed E-index of December-January-February (DJF)-averaged sea-surface temperature anomalies from 1948 to 2023. An EP El Niño is defined when the E-index is greater than 1.0 standard deviation (s.d.) (red circles in **a**) and an EP La Niña when the E-index is greater than -1.0 s.d. in amplitude (yellow circles in **a**). **b,** Same as **a,** but for C-index. A CP El Niño is defined when the C-index is greater than

1.00 standard deviation (s.d.) (purple circles in **b**) and a CP La Niña when the C-index is greater than -1.0 s.d. in amplitude (blue circles in **b**). **c-f,** Composites of 2m air temperature anomalies (shading) for EP El Niño (left), EP La Niña (middle-left), CP El Niño (middle-right) and CP La Niña (right) during July-August-September (JAS; part **c**), October-November-December (OND; part **d**), December-January-February (DJF; part **e**) and March-April-May (MAM; part **f**). Year 0 in parentheses indicates an El Niño developing year and year 1 the subsequent decaying year. Green contours in parts **c-f** represent the 90%, 95% and 99% confidence levels. Stippled areas indicate that more than 70% of events have the same-signed anomalies. Decadal variability not only modulates ENSO impact but also induces decadal anomalies on which ENSO anomalies superimpose, exacerbating interannual anomalies.

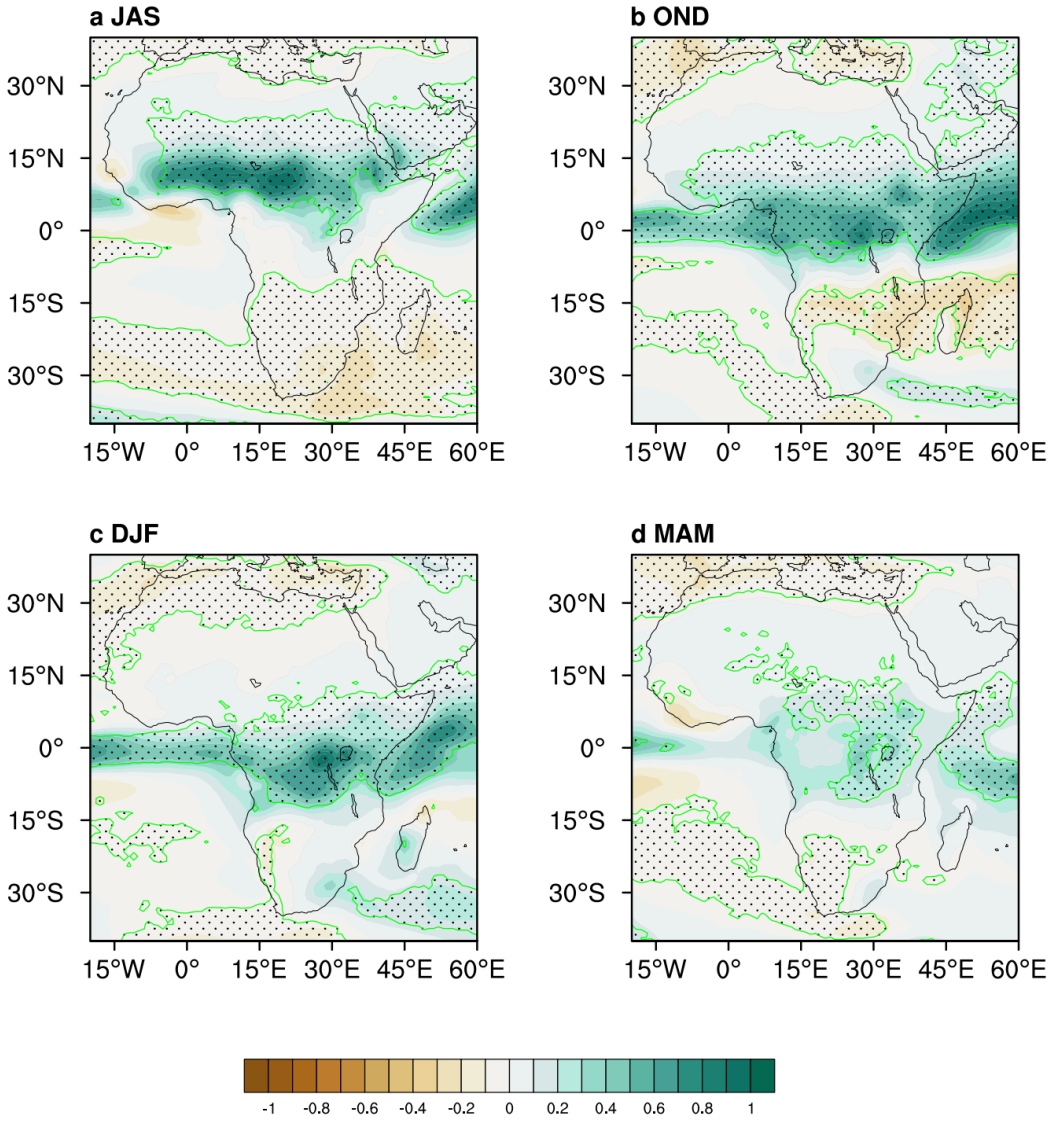

Supplementary Fig. 5 | Mean rainfall change. a, JAS multimodel ensemble mean change of rainfall from 43 CMIP6 models, scaled per degree of warming (mm day^{-1} per

degree of global warming). Stippling and the green contours represent where 80% of the models agree on the sign of the change. **b-d**, as in a but for OND, DJF, and MAM, respectively. Summer rainfall in the Central and East Sahel is projected to increase, as is the short rain in East Africa, but rainfall over southern Africa generally decreases in most seasons.

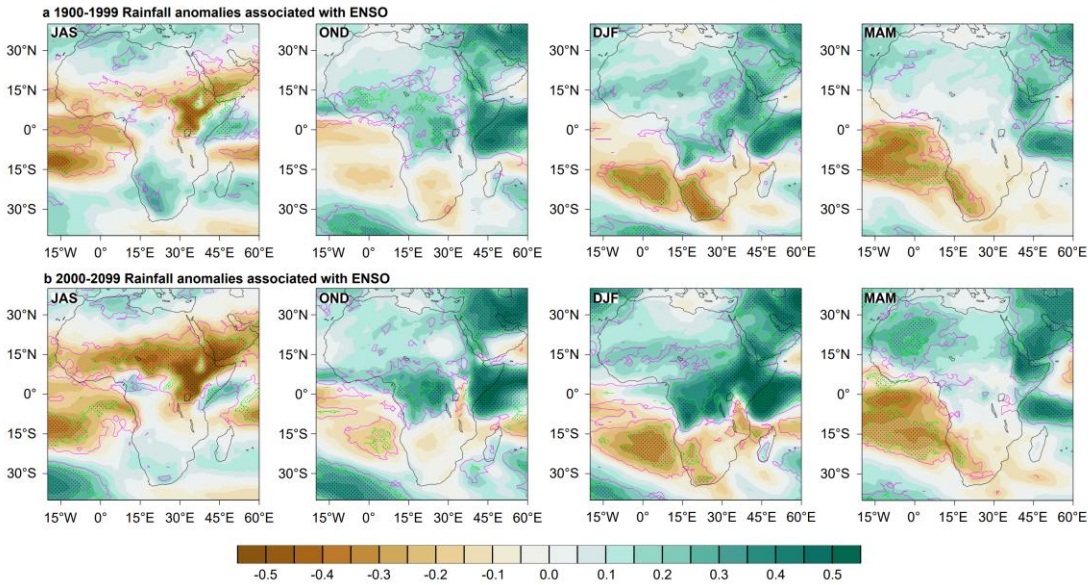

Supplementary Fig. 6 | Future change of African rainfall associated with ENSO in group of 20 models with strongest ENSO nonlinearity. Shown are aggregated over all models. **a, b,** Multimodel ensemble mean of regression (mm day^{-1} ^{o}C^{-1})of rainfall onto Niño3.4 for the 20th and 21st century, respectively, from left to right, in JAS, OND, DJF, and MAM; for each model, for each model, seasonal rainfall anomalies and Niño3.4 are quadratically detrended and normalised over the 1900-2099 period, and then separated into two 100-year periods. Areas confined by purple and green (with stippling) contours indicate where more than 50% and 70% of models agree on a 95% statistically significant correlation, respectively. The intensified ENSO impact under greenhouse warming seen using all models is reproduced in a group of 21 models with highest ENSO nonlinearity.

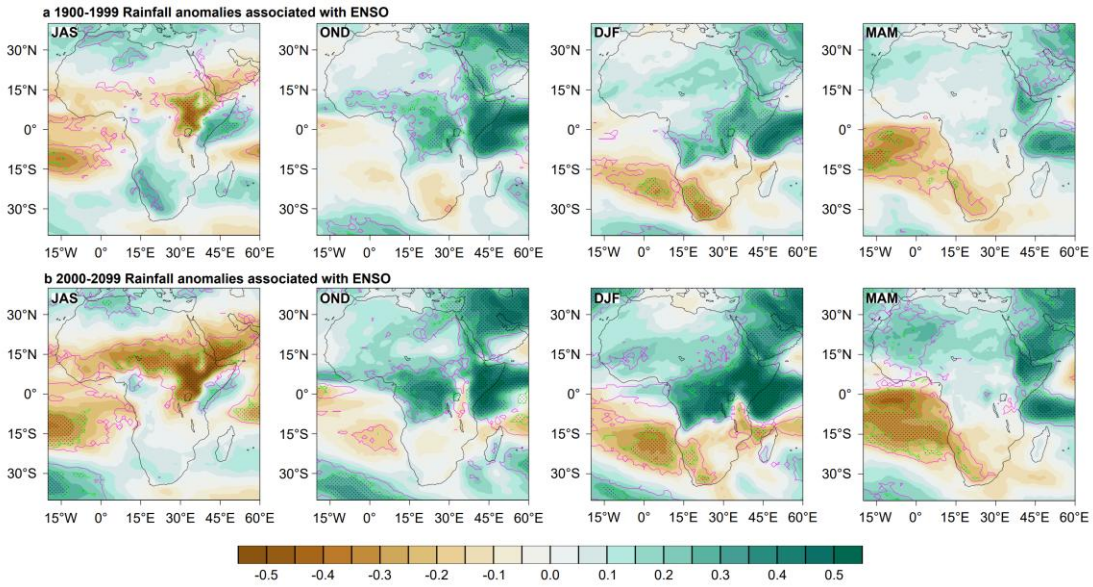

Supplementary Fig. 7 | Future change of African rainfall associated with ENSO in group of 20 models with strongest ENSO-IOD coupling. Shown are aggregated over all models. **a, b,** Multimodel ensemble mean of regression (mm day^{-1} ^{o}C^{-1}) f rainfall onto Niño3.4 for the 20th and 21st century, respectively, from left to right, in JAS, OND, DJF, and MAM; for each model, seasonal rainfall anomalies and Niño3.4 are quadratically detrended and normalised over the 1900-2099 period, and then separated into two 100-year periods. Areas confined by purple and green (with stippling) contours indicate where more than 50% and 70% of models agree on a 95% statistically significant correlation, respectively. The intensified ENSO impact under greenhouse warming seen in ensemble mean across all models is reproduced in a group of 20 models with highest ENSO-IOD coupling.